Ultrasound in Med. & Biol., Vol. 27, No. 5, pp. 695–708, 2001

0301-5629/01/$–see front matter

PII: S0301-5629(01)00342-8

● *Original Contribution*

USE OF OVERPRESSURE TO ASSESS THE ROLE OF BUBBLES IN FOCUSED ULTRASOUND LESION SHAPE *IN VITRO*

MICHAEL R. BAILEY*, LISA N. COURET,* OLEG A. SAPOZHNIKOV,[§] VERA A. KHOKHLOVA,[§] GAIL TER HAAR,[‖] SHAHRAM VAEZY,[†] XUEGONG SHI,[†] ROY MARTIN[†‡] and LAWRENCE A. CRUM*

*Applied Physics Laboratory and Departments of [†]Bioengineering and [‡]Anesthesiology, University of Washington, Seattle, WA, USA; [§]Department of Acoustics, Physics Faculty, Moscow State University, Moscow, Russia; and [‖]Joint Department of Physics, Institute of Cancer Research, Royal Marsden Hospital, Sutton, Surrey, UK

(*Received* 25 *April* 2000; *in final form* 18 *January* 2001)

Abstract—Overpressure—elevated hydrostatic pressure—was used to assess the role of gas or vapor bubbles in distorting the shape and position of a high-intensity focused ultrasound (HIFU) lesion in tissue. The shift from a cigar-shaped lesion to a tadpole-shaped lesion can mean that the wrong area is treated. Overpressure minimizes bubbles and bubble activity by dissolving gas bubbles, restricting bubble oscillation and raising the boiling temperature. Therefore, comparison with and without overpressure is a tool to assess the role of bubbles. Dissolution rates, bubble dynamics and boiling temperatures were determined as functions of pressure. Experiments were made first in a low-overpressure chamber (0.7 MPa maximum) that permitted imaging by B-mode ultrasound (US). Pieces of excised beef liver (8 cm thick) were treated in the chamber with 3.5 MHz for 1 to 7 s (50% duty cycle). *In situ* intensities (I_{SP}) were 600 to 3000 W/cm^2. B-mode US imaging detected a hyperechoic region at the HIFU treatment site. The dissipation of this hyperechoic region following HIFU cessation corresponded well with calculated bubble dissolution rates; thus, suggesting that bubbles were present. Lesion shape was then tested in a high-pressure chamber. Intensities were 1300 and 1750 W/cm^2 (± 20%) at 1 MHz for 30 s. Hydrostatic pressures were 0.1 or 5.6 MPa. At 1300 W/cm^2, lesions were cigar-shaped, and no difference was observed between lesions formed with or without overpressure. At 1750 W/cm^2, lesions formed with no overpressure were tadpole-shaped, but lesions formed with high overpressure (5.6 MPa) remained cigar-shaped. Data support the hypothesis that bubbles contribute to the lesion distortion. (E-mail: bailey@apl.washington.edu)

Key Words: **Lesion, Ultrasound, Cavitation, Overpressure, HIFU.**

INTRODUCTION

Although high-intensity focused ultrasound (HIFU) can be used to necrose tissue deep in the body (Fry et al. 1954; Lynn et al. 1942; ter Haar 1998; Vaezy et al. 2000), treatment is often without real-time feedback on the size, shape and position of the lesion produced. There is concern that changes in HIFU intensity can change the lesion shape (Watkin et al. 1996). The subject of this study was to determine if the formation of gas and/or vapor bubbles contributes to this change in shape.

Several authors (Fry 1993; Lizzi et al. 1986; Lizzi 1993; Sanghvi et al. 1995; Watkin et al. 1996) reported that, as HIFU intensity was increased, the lesion became broader at the end near the transducer and took on the shape of a tadpole, rather than a cigar. Increasingly more of the lesion forms in front of the geometric focus than behind it. Others (Wojcik et al. 1995; Meaney et al. 1998; Curra et al. 1998) found that a finite-amplitude propagation model coupled to a bioheat equation (Pennes 1948) predicted tadpole shapes and movement of the lesion, but not to the degree observed by Watkin et al. (1996). All three groups and Chavrier et al. (2000) also have calculated that gas and/or vapor bubble formation could contribute in large part to the observed distortion and migration.

Experimental evidence exists for suspecting that gas and or vapor bubbles are present during HIFU treatment. Acoustic pressures, commonly 5 MPa *in vivo*, are greater

Address correspondence to: Michael R. Bailey, Applied Physics Laboratory, University of Washington, 1013 NE 40th St., Seattle, WA 98105 USA. bailey@apl.washington.edu

than the cavitation threshold in clean, degassed (although not pure) water (Atchley et al. 1988), and equivalent pressures have been shown to produce cavitation *in vivo* (Holland et al. 1996). Temperatures produced by HIFU and measured *in vivo* are sufficiently high to cause boiling (Clarke and ter Haar 1997; Lele 1986) and/or significant outgassing (Lizzi et al. 1986; Vaezy et al. 2000). B-mode US has shown a hyperechoic region—speculated to be bubbles—at the HIFU treatment site immediately following HIFU (Fry 1970; Fry et al. 1970; Gelet et al. 1993a, 1993b; Lizzi et al. 1986; Sanghvi et al. 1995; Vaughan 1993; Watkin et al. 1995). The hyperechoic region has also been demonstrated when the B-mode image was intermittently synchronized with the HIFU exposure (Vaezy et al. 2000). The hyperechoic region fades with time after treatment. Crum and Law (1995) and Sanghvi et al. (1995) found that, when the hyperechoic region appeared, HIFU transmission was obstructed so that a lesion could no longer be produced beyond the bright region. They also detected subharmonic signals from which they deduced bubbles were present in the hyperechoic region, and proposed that HIFU heated the tissue, forming vapor cavities into which gas could then diffuse. Lele (1986) and Vykhodtseva et al. (1995) have also used subharmonic detection as evidence of bubbles in HIFU. Vaezy et al. (2000) observed real-time movement of the hyperechoic region toward the transducer (0.246 ± 0.09 cm/s) and a corresponding shape change in the lesion. These and other distorted lesions show macroscopic evidence of mechanical damage, pitting and pocking, that has been suspected to be due to cavitation (Vaezy et al. 2000; Watkin et al. 1996).

Given that bubbles may be induced by HIFU, how do they contribute to lesion formation and migration? It has been proposed (Meaney et al. 1998; Watkin et al. 1996) that the heated region and the lesion form in a cigar shape until temperatures are sufficiently high to create bubbles. Elevated temperature increases the vapor pressure of tissue water to the point that boiling and or cavitation occurs. Gas may enter the vapor nuclei because of rectified diffusion and or because the heated tissue becomes supersaturated with gas (Crum and Law 1995). Sound then no longer propagates through the bubble cloud because of the low impedance of gas and/or vapor, and is scattered back toward the transducer. The HIFU energy is, therefore, concentrated in front of the geometric focus and in a somewhat broader pattern. The prefocal region heats preferentially, more bubbles grow and the lesion migrates toward the transducer.

Overpressure—elevated ambient pressure—counteracts the growth of bubbles in three ways. The boiling temperature is raised with overpressure; thus, vapor bubbles are less likely to form. The saturation concentration of gas in water increases; thus, making gas less likely to leave solution and increasing the rate at which bubbles redissolve into solution. Fewer gas bubbles, therefore, form. Finally, overpressure restricts the amplitude of oscillation in bubble radius; thus, reducing the scattering area of bubbles and the amplitude of motion over which the bubbles do work.

Overpressure has been used previously to suppress and assess the role of bubbles in ultrasound (US)-induced biologic effects (Bronskaya et al. 1968; Hill 1971). Lele (1986) did an extensive study of HIFU and overpressure. He and his students found overpressure could suppress wide-band acoustic emission likely from bubbles. They also conducted an experiment much like that reported in this paper. They put *in vivo* tissue under pressure, treated and compared lesion size and shape. Using an intensity of 525 W/cm^2 and a frequency of 2.7 MHz in *in vivo* tissue, they found cigar-shaped lesions were produced at 1 atm (0.1 MPA) or 42 atm (4.2 MPa) hydrostatic pressure.

In the work reported here, changes in boiling temperature, bubble dissolution rate and amplitude of bubble oscillation were quantified numerically. Excised tissue was pressurized to 0.7 MPa and to 5.6 MPa (normal atmospheric pressure is 0.1 MPa). In the low-pressure chamber, B-mode US imaging was used to look for evidence of bubbles. In the high-pressure chamber, differences in lesion shape with and without overpressure were observed and correlated with bubble activity. Acoustic intensities that produced tadpole-shaped lesions at 0.1 MPa were investigated.

Calculations and numerical methods

Overpressure affects bubble formation and activity and, therefore, bubbles' role in distortion of a lesion or appearance in a B-mode US image. The goal of this section is to quantify some of the uniquely strong ways that overpressure affects bubbles. The effects considered are on boiling temperature, outgassing/dissolution rates and bubble dynamics. Increased boiling temperatures associated with higher overpressures means fewer smaller vapor bubbles form. Greater gas solubility associated with increased overpressure means that fewer, smaller gas bubbles exist. Constriction of existing bubbles due to overpressure means that bubbles do not grow as large under insonification. Fewer, smaller bubbles mean less HIFU scattering, which, we propose, produces less distortion of the HIFU lesion. The three effects are coupled, but we will here discuss them separately. The calculations presented are for air and water. Tissue effects have been neglected. First the overpressures used are discussed. Then, quantitative analysis of overpressure effects on bubbles is carried out. Finally, distortion of the acoustic field—and, perhaps, a lessening of other lesion-distorting mechanisms—by overpressure are discussed.

Two elevated hydrostatic pressures were chosen: 0.7 MPa and 5.6 MPa. Pressures quoted are absolute.

They were the maximum obtainable with each of our two pressure chambers. A continuous wave acoustic intensity (I) of 1000 W/cm^2 corresponds to a peak acoustic pressure (p) given by the relationship:

$$I = p^2/2\rho a \tag{1}$$

of 5.7 MPa, where ρ is density of liver (1060 kg/m^3) and a is sound speed (1570 m/s)). The lower pressure chamber gave 7 times the standard atmospheric pressure, but only approximately 1/8th of the peak acoustic pressures used. Little effect would, therefore, be expected when the sound is on. However, the high-pressure chamber exerted pressures comparable to those in the acoustic field and may be predicted to have a significant effect during US exposure.

Overpressure and boiling temperature

Overpressure raises the boiling temperature and, thus, reduces the size and abundance of vapor bubbles produced through HIFU heating. Boiling is the formation of vapor bubbles due to increased temperature and is one way of forming bubbles. Boiling temperatures at 0.1 MPa (standard atmospheric pressure), 0.7 MPa and 5.6 MPa are 100°C, 165°C and 271°C, respectively (Weast 1985). Temperature rises produced by HIFU have not been reported for increased ambient pressures of 0.7 MPa and 5.6 MPa but, at 0.1 MPa, temperatures of 70 to 100°C have been recorded (Clarke and ter Haar 1997; Vaezy et al. 2000) and boiling suspected. Therefore, in the absence of overpressure, vapor bubbles may be formed by boiling the tissue water with HIFU but, with overpressure, vapor bubbles are unlikely to form by this mechanism.

Overpressure and gas diffusion

Overpressure compresses bubbles and increases gas solubility in water; thus, reducing the size and abundance of gas bubbles. In this section, a numerical model of dissolution (or growth) of a bubble, calculated dissolution times t_d as a function of overpressure, and calculations with overpressure and a sudden temperature elevation are presented.

Our model is that proposed by Epstein and Plesset (1950) for a single spherical quiescent bubble in water. No account was made for barriers presented to diffusion by the tissue structure. Other factors may exist to preserve gas bubbles (Akulichev 1966; Apfel 1970; Atchley 1984; Yount 1979), but these are neglected.

The diffusion of gas into or out of a bubble is described by the diffusion equation:

$$\frac{\partial c}{\partial t} + u\,\frac{\partial c}{\partial r} = D\,\frac{1}{r^2}\,\frac{\partial}{\partial r}\left(r^2\,\frac{\partial c}{\partial r}\right) \tag{2}$$

where c is gas concentration in the water, r is radial distance from the bubble center, u is the radial component of the liquid velocity and D is the diffusion constant of the gas in the liquid. The liquid can be considered as incompressible most of the time; this gives an expression for the radial velocity of $u = R^2\dot{R}/r^2$, where R and $\dot{R}$ are the radius and radial velocity at the bubble-water interface. Initially ($t = 0$), the concentration of dissolved gas is uniform and equal to c_i which is expressed as $f = c_i/c_0$, where c_0 is the saturated gas concentration. The value of c_0 is related to the ambient pressure p_0 by Henry's law $c_0 = {k_H}^{-1}\,p_0$, where k_H is a constant. Equation (2) for the dissolved gas concentration $c(r, t)$ must be solved at $t > 0$ and $r > R$. The initial condition is $c(r, 0) = c_i$, the boundary conditions are $c(\infty, t) = c_i$ and $c(R,t) = c_s$, where c_s is the saturated gas concentration in liquid at the bubble interface. According to Henry's law, $c_s = {k_H}^{-1}p_g$, or (neglecting the dependence of k_H on temperature),

$$c_s = c_0 p_g/p_0. \tag{3}$$

where p_g is the pressure inside the bubble. The diffusion of gas from the bubble into the liquid gives rise to bubble dissolution. The bubble radius during its dissolution varies relatively slowly. It is, therefore, possible to put $u = 0$ in eqn (2). The resulting diffusion equation has an analytical solution in the form of a convolution of the corresponding Green's function with the initial distribution of the dissolved gas concentration. The number of moles $n(t)$ of gas in the bubble can be determined from:

$$\frac{dn}{dt} = -4\pi R^2 D \cdot (c_s - c_i) \cdot \left(\frac{1}{R} + \frac{1}{\sqrt{\pi D t}}\right), \tag{4}$$

(Epstein and Plesset 1950). During the slow changes of the bubble size, the gas temperature can be considered as a constant equal to the liquid temperature T_0. The isothermal gas process is governed by the equation:

$$p_g \cdot \frac{4}{3}\,\pi R^3 = n \cdot G T_0, \tag{5}$$

where $G = 8.31$ m$^3 \cdot$ Pa/(mole $\cdot$ K) is the universal gas constant. The bubble radius behavior can be described by the quasistatic equation:

$$p_g = p_0 + \frac{2\sigma}{R}, \tag{6}$$

where σ is the surface tension, and fluid viscosity and vapor pressure have been neglected. Equations (4)–(6) give the following equation for the bubble radius:

$$\frac{dR}{dt} = -K \frac{1 - f + \frac{2\sigma}{p_0 R}}{1 + \frac{4\sigma}{3p_0 R}} \cdot \left(\frac{1}{R} + \frac{1}{\sqrt{\pi D t}} \right), \qquad (7)$$

where $K = GT_0 D k_H^{-1}$. The initial condition is $R = R_0$ at $t = 0$. The right-hand side of eqn (7) has singularities at $t \to 0$ and $R \to 0$ that can be avoided by calculating the value of $\xi = \sqrt{t}$ as a function of R, instead of considering R as function of t. The equation for $\xi = \xi(R)$ follows from eqn (7):

$$\frac{d\xi}{dR} = -\frac{\sqrt{\pi D}}{2K} \cdot \frac{R \cdot \left(R + \frac{4\sigma}{3p_0} \right)}{(R + \xi\sqrt{\pi D}) \cdot \left[R \cdot (1 - f) + \frac{2\sigma}{p_0} \right]}. \qquad (8)$$

The function $\xi(R)$ is to be calculated when the bubble radius changes from $R = R_0$ to $R = 0$ (to the complete dissolution of the bubble). The "initial" condition is $\xi(R = R_0) = 0$.

Equation (8) was solved numerically using a fourth order Runge–Kutta algorithm (Press et al. 1992). The gas was assumed to be air: $D = 2.42 \cdot 10^{-9}$ m^2/s, $k_H = 116200$ N · m/mole, and $\sigma = 0.0725$ N/m. All calculations began with a bubble of initial radius $R_0 = 3$ or 30 μm at $p_0 = 0.1$ MPa and $T_0 = 20$°C in 100% air-saturated water ($f = 1$). At 1 MHz (the lowest HIFU frequency used in this study), the resonant bubble radius in water is 3 μm; the resonant bubble radius in an elastic medium with the same shear speed (100 m/s) as in liver (Frizzell et al. 1976) is 30 μm (Kargl et al. 1998). The resonant bubble size for the imaging frequencies will be slightly less, and strong scattering might be expected both because of the closeness of the wave frequency to the resonance frequency and because of a high concentration of the bubbles. Blood is likely to be saturated with air, although it may have a low concentration of oxygen (O_2) and a high concentration of carbon dioxide (CO_2). Carbon dioxide has a high saturation concentration, which is neglected here because CO_2 is likely to make up less than 5% of the gas content. Other differences between water and blood are neglected in this simple model. Most notably, surface tension is higher in blood and viscosity, which has been neglected, would play a more important role. Vapor pressure (discussed earlier) is neglected in this model.

Overpressure was assumed to have been applied suddenly, without allowing gas diffusion from outside the fluid, or into or out of the bubble. Because the water in the pressure chambers had little surface area in contact with air and pressures were applied in seconds, but maintained for tens of seconds, these assumptions produce negligible error. A change in overpressure was modeled by changing p_0, reducing bubble size by the cube root of p_0 (*i.e.*, the pressure-volume product of the bubble was held constant), and changing c_0 according to Henry's law: c_i was unchanged. In other words, calculations began with $p_0 = 0.1$ MPa, $R_0 = 30$ μm, and $c_0 = 0.872$ moles/m^3; when pressure was increased, for example 7 times, p_0, R_0 and c_0 were changed immediately to 0.7 MPa, $30 \cdot 7^{-1/3}$ μm and $c_0 = 0.872 \cdot 7$ moles/m^3, respectively. Other effects were considered to be secondary and were neglected. In some calculations, it was assumed the HIFU suddenly increased the temperature from 20 to 100°C. Our first-order modeling here involved changing c_0 only. At 0.1 MPa, c_0 is 0.872 moles/m^3 at 20°C and 0.645 moles/m^3 at 100°C (Weast 1985). Henry's law was then used to calculate c_0 at elevated pressure at the corresponding temperature.

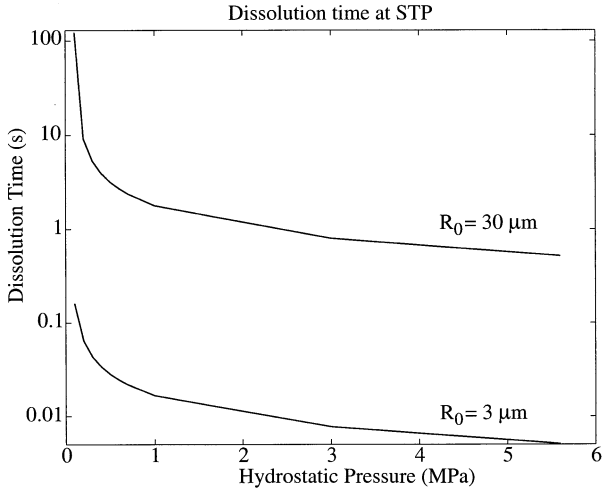

Fig. 1. Time for a 3-μm and a 30-μm bubble to dissolve as a function of hydrostatic pressure.

Figure 1 shows the bubble dissolution time t_d vs. hydrostatic pressure. At standard atmospheric pressure (0.1 MPa), t_d is 0.2 s for a 3-μm bubble and 123 s for a 30-μm bubble. The smaller bubble dissolved more quickly. At higher hydrostatic pressures, the bubbles dissolve more rapidly. At 0.7 MPa, t_d is 0.025 s ($R_0 = 3$ μm) and 2.3 s ($R_0 = 30$ μm). Dissolution time is slow in all cases compared to the period of the acoustic wave. However, treatment times are 1 to 30 s and are comparable to t_d. The assumption of the sudden shrinkage of the bubble associated with rapid pressurization has much less influence on the calculation than the assumption of no change in c_i as a result of sudden pressurization. The drop in t_d due to overpressure primarily results from the change in gas saturation level. In other words, if we

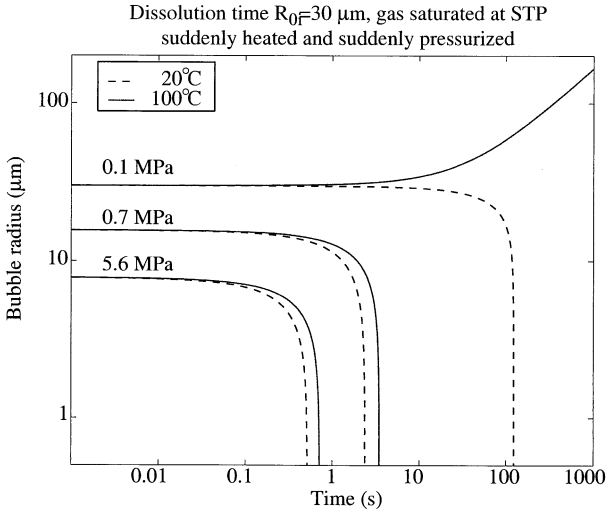

Fig. 2. Bubble radius over time at three hydrostatic pressures and two temperatures. In all cases, the bubble dissolution time (t_d) decreases with increasing hydrostatic pressure. At 0.1 MPa (1 atm) and 100°C, the bubble actually grows because sudden heating causes the water to be supersaturated.

assume a bubble radius of 30 μm not $30{\cdot}7^{-1/3}$ μm at 0.7 MPa, $t_d = 7$ s or if c_i is allowed to equilibrate to $f = 1$ at 0.7 MPa, $t_d = 122$ s. In unsaturated water, the dissolution times are shorter.

Bubble dissolution at 0.1 MPa can be strongly affected by a sudden, HIFU-induced temperature rise and bubbles can grow. Growth occurs because gas solubility decreases with temperature and, thus, with sudden heating, water may become supersaturated. Gas can flow into the bubble instead of flowing out. Figure 2 shows the result of changing the saturation concentration suddenly from that at 20°C to one corresponding to that for water at 100°C and also, where applicable, changing bubble size and c_0 to values appropriate for the overpressure, as done above. Bubble radius is plotted vs. time. Dashed lines show the results at 20°C. At 0.1 MPa, the bubble ($R_0 = 30$ μm) dissolves after 123 s. Overpressure is applied at $t = 0$ s. Therefore, at 0.7 MPa, the bubble is initially smaller ($30{\cdot}7^{-1/3}$ μm) and the bubble has dissolved after 3 s. The solid line represents the calculation made after a temperature rise to 100°C at $t = 0$. The solid lines at 0.7 MPa and 5.6 MPa show a slightly longer dissolution time than their corresponding dashed lines because the saturation concentration is lower at 100°C. At 0.1 MPa, the solid line shows bubble growth because the water is now supersaturated. The effect of overpressure demonstrated in Fig. 2 is very strong. However, the initial concentration of gas in solution must be exact to predict the precise temperature for growth. In addition, growth occurs only after the pressure gradient has overcome surface tension. Smaller gas bubbles (*e.g.*, with $R_0 = 3$ μm) will not grow even at 100°C. Saturation concentration c_0, which drives dissolution or growth, is directly proportional to p and nearly inversely proportional to T. However, a temperature rise from 20°C (293 K) to 100°C (373 K) is a much smaller relative change than the pressure changes that we have considered (0.1 MPa to 0.7 MPa to 5.6 MPa). Secondary temperature effects, such as changes in the diffusivity constant D and Henry's constant k_H and viscosity were neglected.

Overpressure and bubble dynamics

In the static case where the HIFU sound field has not been addressed, overpressure makes the formation of vapor bubbles less likely, and existing gas bubbles more likely to dissolve; thus, reducing the number and size of bubbles. The last consideration is the effect of acoustic pressure fluctuations on the size of the bubble. Large radial oscillations create large scattering targets, but overpressure constrains bubble oscillation.

The model used for bubble dynamics is the Gilmore–Akulichev formulation (Akulichev 1971; Gilmore 1952), with gas diffusion included as described by Church (1989). The Gilmore equation describes the oscillations of a single spherical bubble driven by an acoustic excitation and can be written in the following form:

$$\left(1-\frac{\dot{R}}{a}\right)R\ddot{R}+\frac{3}{2}\left(1-\frac{\dot{R}}{3a}\right)\dot{R}^2 = \left(1+\frac{\dot{R}}{a}\right)H+\left(1-\frac{\dot{R}}{a}\right)\frac{R}{a}\frac{dH}{dt}, \quad (9)$$

where R is the bubble radius, a dot indicates a time derivative, t is time, a is the speed of sound in the liquid at the bubble wall, and H is the difference in the liquid enthalpy between the bubble wall and infinity. The expressions for:

$$a = \sqrt{dp/d\rho} \quad (10)$$

and

$$H = \int_{p_\infty}^{p(R)} dp/\rho \quad (11)$$

were obtained from the Tait equation of state for the liquid (Sullivan 1981; Thompson 1988):

$$p = p_0 + (a_0^2\rho_0/\Gamma)\cdot[(\rho/\rho_0)^\Gamma - 1], \quad (12)$$

where Γ is the Tait parameter, p_0 is ambient pressure, ρ_0 ambient density and a_0 small-signal sound speed (Church

1989). The upper limit of the enthalpy integral is the pressure at the water-gas interface (*i.e.*, the bubble wall $p(R) = p_g - 2\sigma/R - 4\mu\dot{R}/R$, where p_g is the pressure in the gas, given below, σ is the coefficient of surface tension and μ the coefficient of shear viscosity). The lower limit $p_\infty = p_0 + P(t)$ is the pressure at infinity, where $P(t)$ is acoustic pressure produced by the HIFU source.

Gas diffusion was calculated using a zero-order model for gas diffusion based on the theory by Eller and Flynn (1965). Because the radius changes very quickly, eqn (8) is not appropriate. The number of moles of gas *n(t)* in the bubble is given by the following equation:

$$n = n_0 - 4\sqrt{\pi D}\int_0^\tau F(\tau')(\tau - \tau')^{-1/2}d\tau', \quad (13)$$

where n_0 is the initial number of moles in the bubble, $F = c_0(p_g/p_0) - c_i$, $p_g = (p_0 + 2\sigma/R_0) \cdot (n/n_0) \cdot (R_0/R)^{3\gamma}(R_{0n}/R_0)^{3(\gamma-1)}$ is the pressure in the gas, R_{0n} the time varying equilibrium radius, γ is the adiabatic exponent of the gas, and

$$\tau = \int_0^t R^4(t')dt'. \quad (14)$$

Equation (13) follows from a first-order approximation solution to eqn (4). The bubble may, in fact, grow while oscillating (Eller and Flynn 1965).

Figure 3 shows the radius vs. time curves created by a 30-cycle, 1-MHz, 5-MPa HIFU pulse at three hydrostatic pressures. Radius is on a log scale. The maximum radii (R_{max}) and the ratios of R_{max} to the minimum radius R_{min} are listed in Table 1. These calculations again assume the same size bubble at 0.1 MPa and that the bubble shrinks when pressure is increased. At 0.1 MPa, the bubble oscillations reach the largest R_{max}, the ratio R_{max}/R_{min} is the greatest, and oscillation continues for the longest time. The slow ringing decay (~20 cycles) seen at 0.7 MPa also occurs at 0.1 MPa, but was cropped from the figure. Absolute values of R_{max}, R_{max}/R_{min}, and duration vary with initial radius R_0 and frequency, but the inverse relation between overpressure and amplitude and duration of oscillation was robust (even for the unrealistic case where the bubble does not shrink but, instead, takes in sufficient gas to maintain its size when pressure is applied). Thus, bubbles do not grow as large under overpressure.

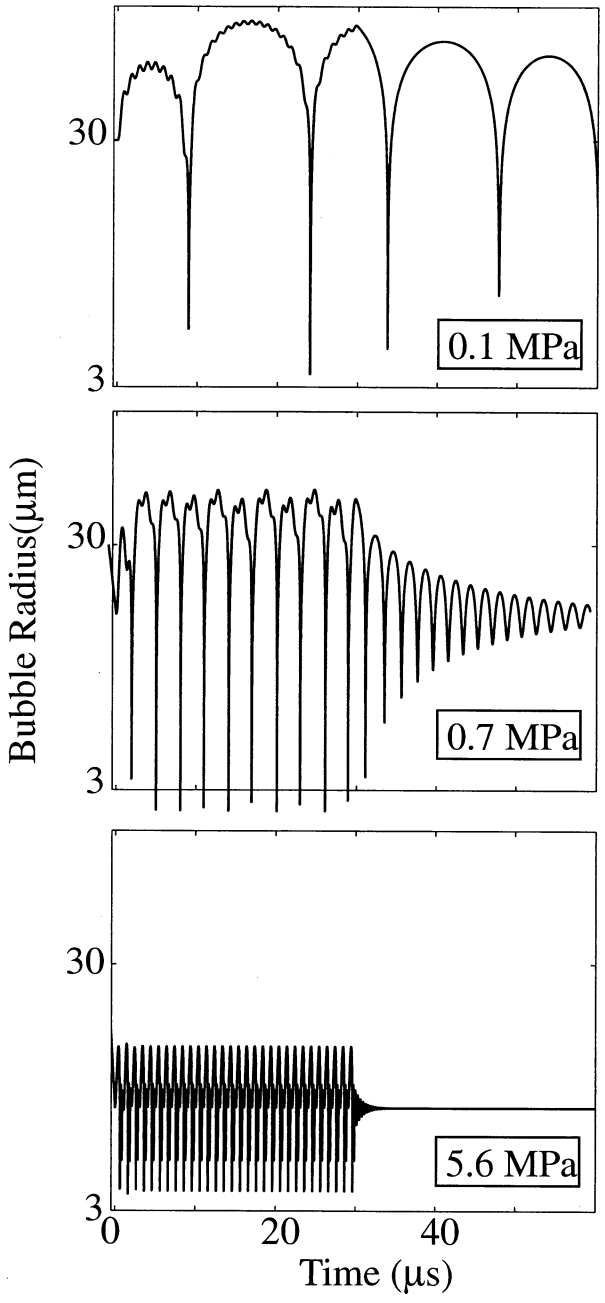

Fig. 3. Bubble radius as a function of time for three hydrostatic pressures. Initial bubble radius at STP is 30 μm, peak HIFU acoustic pressure is 5 MPa, and HIFU frequency is 1 MHz. Maximum bubble radius and duration of bubble activity are inversely proportional to hydrostatic pressure.

Overpressure and nonbubble mechanisms

The above calculations indicate that overpressure reduces the presence of bubbles in HIFU imaging and lesion formation. A pressure change from 0.1 MPa to 5.6 MPa caused the boiling temperature to increase 45% ($|544 - 373$ K$|/373$ K), our calculated dissolution time to decrease 99% ($|0.5 - 123$ s$|/123$ s), ingassing due to temperature never to occur, and the amplitude of

Table 1. Maximum radius R_{max} and ratio R_{max}/R_{min} of maximum to minimum radius calculated in Fig. 3

Hydrostatic pressure (MPa)	R_{max} (μm)	R_{max}/R_{min}
0.1	91.8	27.2
0.7	50.5	20.6
5.6	14.2	4.1

bubble oscillation to decrease 85% ($|4.1 - 27.2|/27.2$). There is little reason to suspect that overpressure produces similarly large changes in other physical properties that might influence HIFU imaging and lesion formation. Changes in the ability of the transducer to generate the sound in the medium, alteration of the acoustic properties of the medium and differences in the absorption and conversion of sound to heat are considered here.

The strain constants, permittivity and dielectric loss of a piezoceramic transducer (PZT—4), material parameters responsible for the acoustic output, change less than 1% between overpressures of 0.1 MPa and 5.6 MPa (Nishi and Brown 1964). This change was considered negligible. For verification, the complex electrical impedance of our transducer was measured on an impedance analyzer (HP 4192A Hewlett Packard, Palo Alto, CA). The frequency-dependent impedance measured with the transducer at 5.6 MPa did not differ significantly ($n = 3$) from that measured at 0.1 MPa. Standard deviations in the measurements were less than 5%. The acoustic output was, therefore, the same for the high- and low-pressure experiments.

The acoustic impedance ($z = \rho a$) is the primary descriptor of the acoustic properties of the medium. Although z has not been reported for tissue as a function of pressure, the sound speed in water (and most other liquids and solids) changes very little, <1% for pressure changes from 0.1 MPa to 5.6 MPa (Medwin 1975). By definition, sound speed is $a = \sqrt{dp/d\rho}$, which can be rewritten as $d\rho = dp/a^2$ to evaluate the density change. Inserting $dp = 5.5$ MPa and $a = 1500$ m/s yields a 0.2% change in density ($\rho_0 = 1000$ kg/m^3). Thus, a 5.5-MPa increase in pressure increases acoustic impedance in water by less than 1%. If we assume tissue is not too dissimilar to water, this means that the acoustic properties are unaltered between our high- and low-pressure experiments.

Absorption, a primary part of attenuation α, and nonlinearity, summarized in the coefficient β, are material properties that affect the conversion of acoustic energy to heat, which is a major mechanism in lesion formation. The effect of overpressure on these properties in tissue is not known; however, a comparison of the amplitude and frequency content of waveforms measured at 0.1 MPa and 0.4 MPa indicates little difference in absorption or nonlinearity.

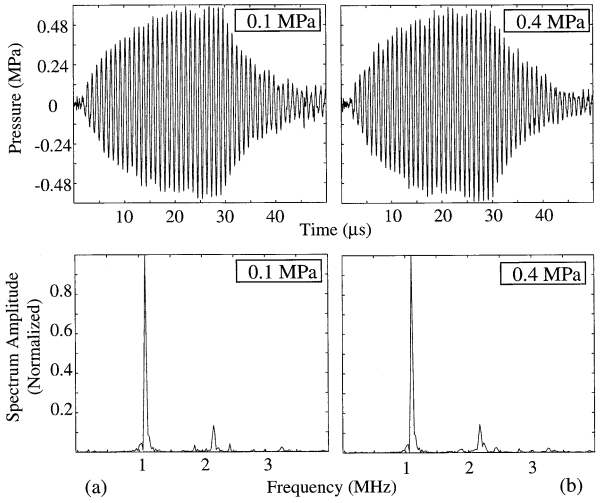

Fig. 4. Pressure waveforms and frequency spectra measured across liver pressurized to (a) 0.1 MPa and (b) 0.4 MPa.

Figure 4 shows the waveforms and the Fourier transforms of the waveforms. Waveforms were measured using a PVDF membrane reference shock wave hydrophone (Sonic Industries (SI), Hatboro, MA) in water. The geometric diameter of the sensitive element was less than 0.5 mm. The source was an air-backed, concave, single element, PZT-4 piezoceramic transducer (Cleveland et al. 2000) with 20-cm focal length, 10-cm aperture, and 1.08-MHz resonance frequency. Between source and receiver was placed pressure chamber 1 (Fig. 5) so that the sound passed through a cylinder (10.6-cm diameter) of excised beef liver and the polyethylene terephthalate (PETE) walls of the chamber. The cylinder was 1 mm away from the hydrophone to minimize shock-wave healing in the water bath. Five measurements were made after 2 min at 0.4 MPa and then 2 min and 10 s later at 0.1 MPa. The process was repeated for three different specimens of tissue. Waveforms were transferred from the Tektronix TDS 744A digitizer (100 MS/s) to the Macintosh G3 *via* LabVIEW (National Instruments, Austin, TX). The Fourier transform was taken of the waveforms using the canned algorithm in MatLab (Natick, MA) without additional windowing. The mean of the peak amplitudes of the waveforms ($n = 15$) was 0.37 ± 0.06 MPa at 0.1 MPa and 0.39 ± 0.03 MPa at 0.4 MPa. The mean of the ratios of second harmonic amplitude to fundamental amplitude was 0.14 ± 0.01 at 0.1 MPa and 0.12 ± 0.03 at 0.4 MPa. Differences in amplitude and frequency content were not statistically significant.

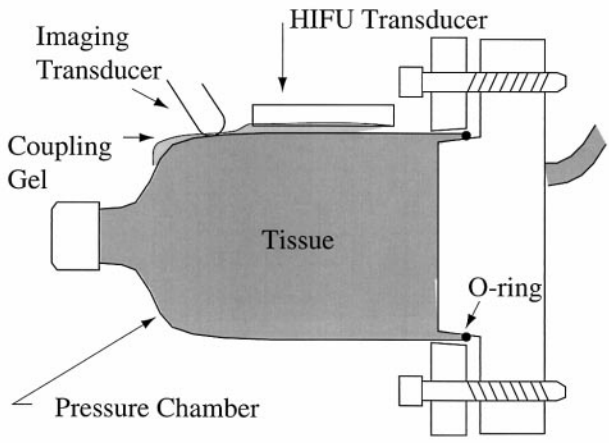

Fig. 5. Schematic diagram of experiments in chamber 1.

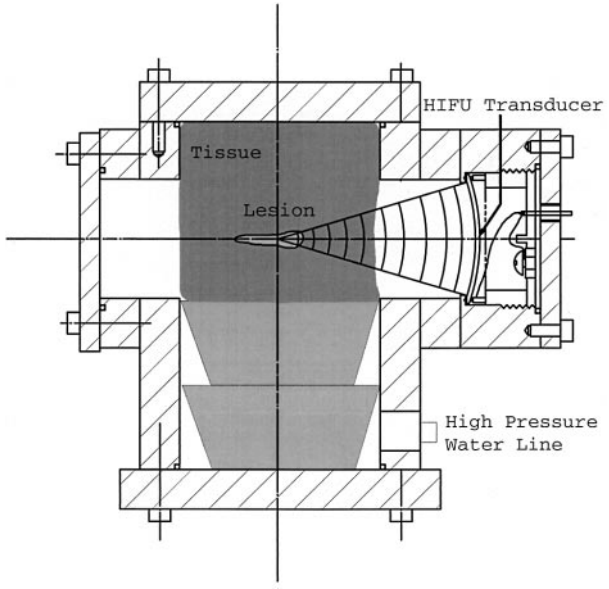

Fig. 6. Schematic diagram of experiments in chamber 2.

There may be other factors, possibly biologic or chemical changes, that the authors have overlooked, but it seems probable that overpressure's effect on bubbles far outweighs its effect on acoustic parameters that might affect the shape of the lesion.

Experimental materials and methods

Each experiment consisted of exposure of freshly excised beef liver to HIFU with and without overpressure. Whole beef liver was obtained on the day of the experiment from Schenk Packing Co. (Stanwood, WA). Each liver was excised within 20 min of animal euthanasia and stored in a plastic bag at room temperature. Pieces of liver were cut to fill one of the two pressure chambers shown in Figs. 5 and 6. The chambers were designed and positioned so that the ultrasonic beam was always incident on the sample through the liver capsule.

Experiments in chamber 1 (Fig. 5) utilized a 3.5-MHz HIFU therapy transducer (Sonic Concepts, Woodinville, WA) that had an aperture diameter of $d = 35$ mm, and a focal depth $F = 55$ mm. Experiments in chamber 2 (Fig. 6) utilized a 1-MHz therapy transducer in which $d = 40$ mm and $F = 64$ mm. The element was manufactured at Channel Industries, Santa Barbara, CA, and the transducer was designed and assembled at the California Institute of Technology. Both transducers employed air-backed, concave, single PZT-4 elements. Each therapy transducer was driven using a function generator (33120A, Hewlett Packard, Palo Alto, CA) and amplified by an AP400B (used with pressure chamber 1 described below) or an A300 (chamber 2) power amplifier (ENI, Rochester, NY). Custom-built electrical networks matched the transducer to a 50-Ω load. Forward power to the matching network was monitored by the gauge on each amplifier.

Both transducers were calibrated in deionized, degassed water with the reference shock wave hydrophone, the Tektronix digitizer, and LabVIEW Software. The half-maximum focal beam length and width were mapped at low power and are presented in Table 2. The pressure output of the 3.5-MHz transducer and the AP400B amplifier and the 1-MHz transducer and the A300 amplifier were measured in degassed, deionized water. Three repeat measurements of a 10-cycle burst and of 10 cycles near the end of a 500-cycle burst were averaged. As long as the water was degassed and the AB400B amplifier was unleveled, no significant difference was seen between the short and long burst waveforms. The intensity at the focus was calculated using eqn (1) where pressure p equals the average of the peak positive and negative pressures.

In situ intensities were calculated assuming a 3-cm path through liver. The rest of the axial path was water, for which losses were neglected. An attenuation coefficient of 0.05 Np/cm/MHz was used and gives the value 0.73 dB/cm at 1.7 MHz (Pohlhammer et al. 1981) used by Watkin et al. (1996). We have measured a similar value 0.037 Np/cm/MHz *in vivo* in pig liver (Vaezy et al. 2000). Duty cycles were 50% at 3.5 MHz and 100% at 1 MHz. At 3.5 MHz, the *in situ* spatial peak intensities (I_{SP}) used were 600 to 3000 W/cm^2 (I_{SPTA} values are half because of the 50% duty cycle), and *in situ* acoustic pressure amplitude p was 4.2 to 9.5 MPa. Results presented are for 1500 W/cm^2 and 6.7 MPa. At 1 MHz, the *in situ* intensities used were 1300 and 1750 W/cm^2 ($\pm$ 20%), and derated pressures were 6.2 and 7.2 MPa ($\pm$ 10%). The hydrophone was calibrated by the manufacturer to within $\pm$ 10% (Sonic-Technologies 1994).

Table 2. Comparison of transducers

Frequency (MHz)	Focal distance (F, mm)	Aperture radius (d/2, mm)	Half-max beam length (mm)	Half-max beam width (mm)	Duty cycle (%)	Use
3.5	55	17.5	9	1	50	chamber 1
1.0	64	20	36	3.3	100	chamber 2
1.7	150	42	19.5	1.65	100	Watkin et al. (1996)

The low overpressure chamber (Fig. 5) was constructed from a polyethylene terephthalate (PETE) soda bottle (Bailey et al. 1999) with a flange. The bottle bottom was removed with scissors and then press fit by hand over a beveled aluminum platform in the base. An O-ring was trapped between the bottle and platform. A complementary beveled ring slid over the bottle and was bolted to the aluminum base. As the bolts were tightened, the lip of the bottle became more tightly pinched between ring and platform. The chamber was pressurized with a water-filled hand pump (Ralston Instruments, Chagrin Falls, OH) to up to 0.7 MPa (0.6 MPa gauge pressure) and, in some cases, depressurized before HIFU exposure. The chamber was placed in a water bath, and throughout deionized water degassed under vacuum according to IEEE Std 790 to 1989 B7 was used. Therapy ultrasound (3.5 MHz, 50% duty cycle, 300 to 1500 W/cm^2 *in situ*, 1 to 7s) was applied through the PETE wall of the chamber. There was 90% pressure transmission through the PETE as determined in water with the SI hydrophone, and calculations of *in situ* intensities and pressures were adjusted accordingly.

A confocal imaging probe (C9–5 ATL, Bothell WA) was used to make B-mode images of the HIFU field on an ATL HDI 3000. Imaging and HIFU were synchronized to a 50% duty cycle of HIFU on a roughly 1/30th s period so that scattering of the HIFU did not "white out" the B-mode image (Vaezy et al. 2000). US images were recorded on video tape and, after each experiment, digitized on a Macintosh G3. The size of the hyperechoic region was measured from the digital images, and the time of its existence was recorded by an observer blind to the exposure conditions. The time of existence was measured by taking the grey-scale pixel histogram of the region surrounding the hyperechoic region. Truly white pixels appeared in this region only after HIFU treatment. The disappearance of the white pixels was used as the endpoint for when the image had dissipated.

The high overpressure chamber (Fig. 6) comprised two short, hollow, steel cylinders welded to a main cylinder. The end caps on the main cylinder were polyphenylene oxide (PPO) and were bolted on with an O-ring in between. A metal cover bolted over one short cylinder, and the 1-MHz transducer bolted over the other cylinder. Rubber stoppers and degassed water filled the space below the liver specimen. Degassed water filled the space in the smaller cylinders. Liver filled the upper region of the main cylinder. Pressure was applied from a cylinder of pressurized nitrogen gas. The gas line (6.4 mm i.d.) was split into a "T". Gas met with water in the line going to the inside of the chamber, with oil in the line pressurizing the back side of the transducer. The equalized pressure prevented the PZT transducer element from cracking. Unlike chamber 1, for which the transducer was outside the chamber, the transducer operated within chamber 2 while under pressure, albeit being subject to equal pressure across the transducer's PZT element. Overpressure did not change the forward power (as measured on the gauge of the ENI A300 amplifier) to the transducer. In the results presented here, each piece of liver was pressurized to 5.6 MPa for 3 min. The system then either remained at the overpressure and was exposed for 30 s or was depressurized to 0.1 MPa and, after 2 min, exposed for 30 s. This way, gas that may develop in *ex vivo* tissue due to autolysis but that is unlikely *in vivo* could be dissolved and minimized by the overpressure before treatment. The HIFU (1 MHz, 100% duty cycle, 1300 or 1750 W/cm^2, 30 s) was focused at the center of the main cylinder of the chamber (3 cm deep in the tissue).

No B-mode US imaging was done in chamber 2. The lesions formed were analyzed by macroscopic examination after treatment as described by Watkin et al. (1996). The liver sections were placed in a ring with the same diameter as the chamber to confine the tissue as it was in the chamber, and the lesions were measured. Digital photographs were taken of the liver and a reference scale. The images were opened on a Macintosh G3 in Adobe Illustrator (Adobe Systems, Inc., San Jose, CA), and their outlines traced. Tracings were then filled and opened in Adobe Photoshop. The images were divided at the centerline (at half the total length), and distortion of the lesion into a tadpole shape was quantified as the number of pixels in the near half over the number of pixels in the far half. Number of pixels corresponded directly to area. A lesion symmetrical about the centerline, such as a cigar shape, had pixel ratio *PR* of 1 where as the *PR* greater than 1 indicated enlarging of the lesion on the side near the transducer. The centerline had to be used as a reference because the position of

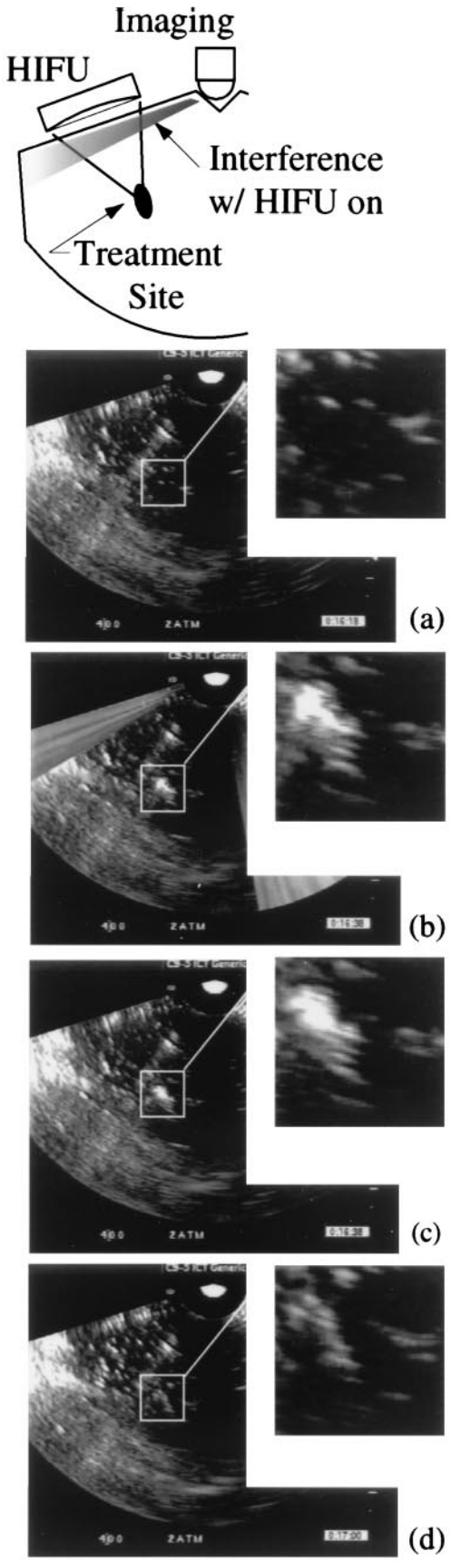

the geometric focus could not be determined precisely. For the same reason, migration of the lesion could not be assessed. The liver, as it was mounted in the chamber, could vary in thickness by up to 2 mm and, therefore, the measurement of the distance from the lesion to the liver capsule was not a precise measure of migration. Lesion tracings and measurements were made by an observer who was blind to the conditions of the experiment.

The transducers in the two chambers differed from each other and from the transducer used in the work by Watkin et al. (1996) that motivated this work. Table 2 compares our two transducers and that of Watkins and colleagues. Higher frequencies and greater focusing (*d/F*) generally cause greater heating and, therefore, require less time to create a lesion. Although use of the same transducer might have made comparison easier, it was not feasible to try to replicate the large transducer of Watkin and colleagues or even to utilize the same transducer with both chambers. Each system was built around an individual transducer, and they could not be interchanged. Nevertheless, our goal was to investigate if suppressing bubble activity with overpressure would reduce the distortion of a HIFU formed lesion. This mechanism is general to HIFU therapy, and independent of the HIFU field or transducer.

RESULTS

No significant difference in size of the hyperechoic region, pressure threshold at which it formed, time to formation or rate of growth was observed between hyperechoic regions measured at 0.1 MPa and 0.7 MPa. The similarity might be expected because both 0.1 MPa and 0.7 MPa are small compared to the HIFU acoustic pressures. However, once the HIFU exposure ceased, the rate of dissipation was greatly affected by overpressure.

Figures 7 and 8 show results obtained with chamber 1. Figure 7 shows a schematic diagram and a time sequence of the hyperechoic region produced by HIFU and detected by B-mode US. The therapy US beam is incident from the upper left of the B-mode sector scan. A box encloses the region where the focused energy creates a hyperechoic region. In (a) before the HIFU is turned on ($t = -15$ s), the box contains small light speckles, but no white pixels. In (b), when the HIFU sound is on ($t = 5$ s), which is indicated by the interference on the outer edges of the sector, the hyperechoic region has appeared. The region has an irregular shape. In real-time, the region can be seen to grow mostly toward the transducer, but to also

Fig. 7. Schematic diagram and time sequence of hyperechoic region in B-mode US image.

get wider. The edges flicker as new small white clumps appear and others disappear. When the HIFU ceases in (c) (t = 5.5 s), the hyperechoic region remains, but begins to dissipate. In (d) (t = 27 s), the image has dissipated so that no truly white pixels remain, although a light haze still exists. Hydrostatic pressure was 0.3 MPa.

Figure 8 shows as a function of overpressure amplitude, a plot of the time for the hyperechoic region to dissipate following cessation of HIFU. The solid line is the mean of 5 measurements and bars mark the standard error. The dissolution time falls from 129 ± 25 s at 0.1 MPa to 1.3 ± 0.2 at 0.7 MPa. The calculated time for a 30-μm bubble to dissolve at each pressure is plotted with a dashed line. Agreement between the values and between the trends of the two curves is good. The strong white backscatter, the appearance of many clustered units in the region, and the correlation between dissipation and dissolution are suggestive that bubbles are created in the HIFU field.

Lesion size measured from the B-mode image agreed well with lesion size measured upon gross histology. Figure 9 shows an example comparison; a photograph of a whitened tadpole-shaped lesion surrounded by dark tissue is on the left and the image of the lesion is on the right. Each measurement method was repeatable to within 10%. Variation in the image was caused by difficulty separating the hazy edge of the lesion from speckle. Variation in the measured histology is due to the flexible, distensible nature of the tissue. The mean difference (n = 26) between image- and histology-based measured length was 17 ± 13% (lengths were 4 to 23 mm) and measured width was 20 ± 20% (widths were 1 to 9 mm). The sample SD is the variation in the percentage difference between the two measurement methods. Image lengths were measured from the outer bounds seen over the time of the image creation. In many instances, the image propagated toward the transducer and, in some cases, hyperecho disappeared behind the advancing front. The image-based length underestimated the histologically measured length 20 of 26 times, but the width was overestimated 15 of 26 times. Two factors were suspected here. First, the length often contained a long thin tail, such as seen in Fig. 9. The thin tail was more difficult to discern from speckle, and the imaging plane had to be precisely aligned to detect the tail. Second, width was measured along the direction of propagation of the imaging sound beam (HIFU was nearly perpendicular to the imaging beams), which appeared to produce hyperechoic artefact (sometimes long streaks along the beam) that made the lower edge of the width difficult to define. We speculate that multiple reflections within the bubble cloud yielded time-delayed echoes interpreted by the imager as originating deeper in the

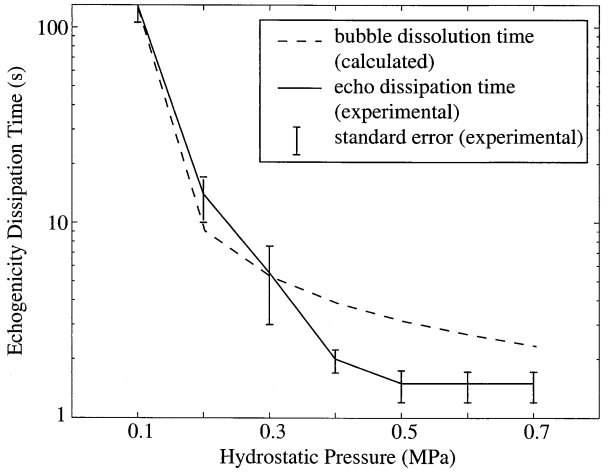

Fig. 8. Measured time for hyperechoic region on B-mode image to dissipate as function of hydrostatic pressure. Both the trend and absolute values compare well to the time calculated for a 30-μm bubble to dissolve.

tissue. Image-based and histology-based measures of the location of the lesion agreed with an average difference of 25 ± 20%. The flexibility of the liver was the major source of variation here. The results include 10 *in vivo* experiments that were done in pig liver where blood perfused the tissue (see the paper by Vaezy et al. 2000 for description of the protocol). Imaging accuracy, compared to histology, did not appear to correlate with HIFU intensity, hydrostatic pressure or tissue perfusion.

Figures 10 and 11 show results obtained with chamber 2. Figure 10 is a photograph comparing lesions formed at 0.1 MPa and at 5.6 MPa. The top of the picture shows the end nearest the HIFU transducer. The lesion is

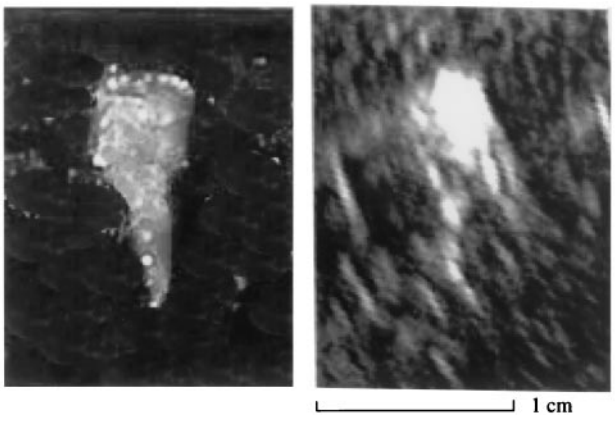

Fig. 9. Comparison of lesion and image produced at 0.1 MPa. The lesion is whitened, with dark tissue surrounding it. The B-mode image is white surrounded by black. Both lesion and image show the same size and tadpole shape.

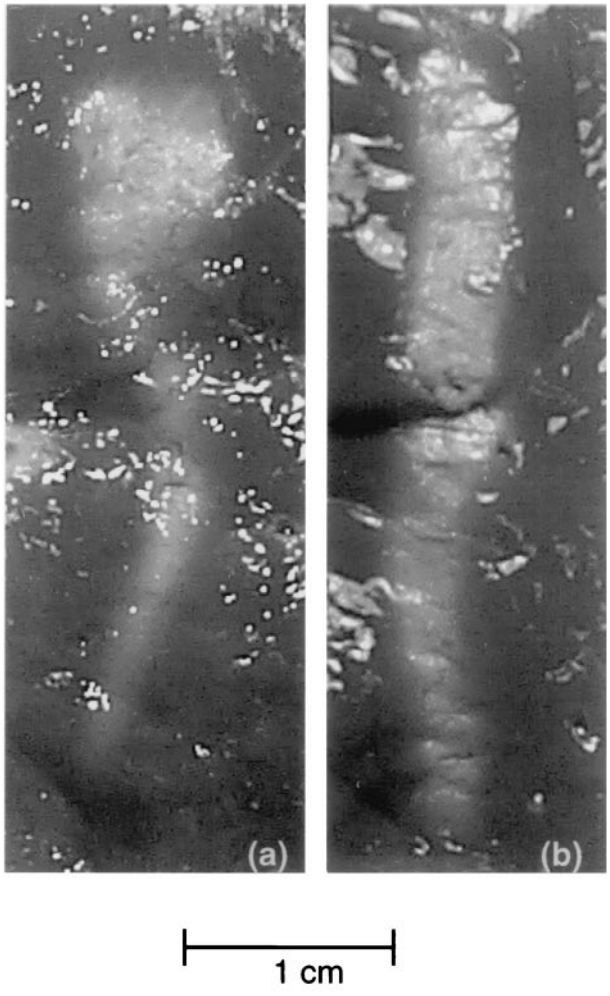

Fig. 10. Photograph of lesions formed at hydrostatic pressures of (a) 0.1 MPa and (b) 5.6 MPa. Each lesion is white with dark tissue surrounding it. Photograph (a) has a "tadpole" shape, and (b) has a "cigar" shape.

the whitened area. The surrounding dark tissue, which had been excised before treatment, does not appear on gross examination to have been altered by the HIFU. The HIFU peak pressure was 7.2 MPa (I_{SPTA} = 1750 W/cm^2), and the time of exposure was 30 s. At 0.1 MPa, the lesion is "tadpole-shaped" and at 5.6 MPa the lesion formed is "cigar-shaped." At lower acoustic intensity (I_{SPTA} = 1300 W/cm^2, p = 6.2 MPa) both lesions were cigar-shaped.

Figure 11 shows the traced perimeters of lesions formed at (a) 0.1 MPa and (b) 5.6 MPa. The shapes in (a) are more distorted and more tadpole-shaped than the shapes in (b). When the lesions are split at the midpoint of their length, the ratio *PR* of the area of the top section to that of the bottom section is 1.7 ± 0.3 in (a) and 1.2 ± 0.2 in (b). The ratios differ significantly (Student's *t*-test,

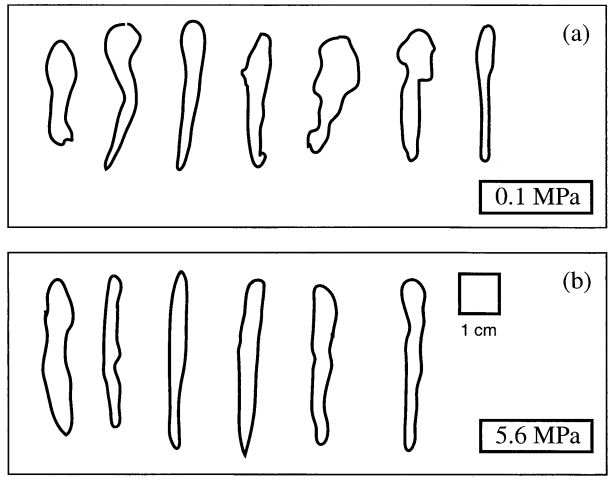

Fig. 11. Perimeters of lesions formed at (a) 0.1 MPa and (b) 5.6 MPa. Shapes in (a) are more distorted and more tadpole-shaped than the shapes in (b).

t = 3.1, p = 0.010). The addition of overpressure reduced the distortion of the lesions into tadpole shapes.

The area ratio is 1.8 ± 0.2 for the second figure and the top three liver lesion shapes in the ninth figure of the paper by Watkin et al. (1996). Our ratios and those of Watkin and colleagues are similar at 0.1 MPa. An area ratio of 1.2 can be calculated from the fourth figure of the paper by Curra et al. (1998) and from the fourth figure (highest intensity curve) of the paper by Meaney et al. (2000). Their figures are for temperature contours produced by a finite-amplitude HIFU wave. Their codes neglected bubbles in these calculations and our experiment at 5.6 MPa suppressed bubbles. The resulting area ratios are similar.

DISCUSSION AND SUMMARY

Numerical results

Good agreement was seen in Fig. 8 between the calculated dissolution time t_d for a 30-μm bubble in water and the dissipation time for the hyperechoic region produced by HIFU in tissue. The t_d calculations are sensitive to the concentration c_i of the gases in solution, which may be measured, and the initial radius R_0 of the bubble, which is not known. Given c_i, we propose that a curve such as presented in Fig. 8 might be used to estimate the size of bubbles created in HIFU or, at least, the size of the bubbles created in HIFU and detected on B-mode US. Our calculations are for a single bubble; break-up, agglomeration or the presence of many bubbles has not been considered. However, in all the calculations, bubble radius is crucial to modeling the interaction of HIFU and bubbles.

The slope is less for the calculations than for the measurements in Fig. 8. Our calculations at low overpressure appear to underestimate the dissolution time (t_d) and, at higher overpressure, overestimate t_d, which might be interpreted as we underestimate the initial size of the bubbles at low pressure and overestimate at high pressure. Times were calculated by assuming insonification had ceased, and the bubble quiescently dissolved. Agreement might be improved by modeling the bubble dynamics under the relevant pressure (Fig. 3) before calculation of bubble dissolution (Figs. 1, 2, 8), because bubbles may grow more by rectified diffusion at low overpressure than at high overpressure. Rectified diffusion is the pumping of gas into the bubble due to the radial oscillation of the insonified bubble (Crum 1982; Eller and Flynn 1965), and we found that the amplitude of bubble oscillation is inversely proportional to overpressure (Fig. 3). It is noted that the bubble dynamics, not only the amplitude of oscillation, vary with overpressure as seen in Fig. 3. For example, the 0.7-MPa curve shows one collapse every 3 acoustic cycles, which is pulsation at the 1/3 subharmonic. The code's calculation of rectified diffusion and vapor pressure can be improved and must remain integrated with the calculation of the bubble dynamics.

Visualization with B-mode ultrasound

A light haze remained on the B-mode US image after the truly white pixels disappeared. This haze did not show a dependence on pressure and persisted for 10 to 20 s. The haze was not observed at low overpressures, where the white pixels persisted longer than 20 s. This haze, perhaps, indicates that a second and yet undefined mechanism contributes to US visualization. The ability to eliminate bubble formation and continue to visualize the treatment site may lead to guided and controlled HIFU therapy.

Macroscopic studies

Watkin et al. (1996) observed mechanical damage, pitting and pocking, in the tadpole-shaped lesions. These lesions, they called "bubbly." We observed a small number of pits and pocks in our experiments at both 0.1 and 5.6 MPa. No method was devised to quantify the pitting; however, it demonstrates that 5.6 MPa of hydrostatic pressure did not completely suppress cavitation produced by 30-s HIFU exposures at peak acoustic pressures of 7.2 MPa. A higher pressure chamber with the ability to image with B-mode US will be used to investigate if cavitation can be suppressed completely.

Clinical relevance

Growth, distortion and migration of the hyperechoic region were seen with B-mode US in our experiments, which leaves the potential for real-time assessment of lesion distortion *in vivo*. Our experiments were conducted *in vitro*, and the cavitation suppression methods must be tested *in vivo* as well. We have observed that the hyperechoic region dissipates more quickly *in vivo* than *in vitro*; we presume because perfusion washes away bubbles *in vivo* (Vaezy et al. 2000).

Our goal was not to introduce overpressure to control lesion shape in clinical treatment, but to use overpressure to better understand the mechanisms (particularly bubble formation) responsible for lesion distortion. Other methods may be used to emphasize or to de-emphasize bubbles' role in clinical treatment. Here, we found that overpressure, which suppresses the formation and growth of bubbles, reduces the distortion in the shape of the lesion.

CONCLUSION

Overpressure or increased hydrostatic pressure was used to assess the role of bubbles in distortion of a tissue lesion produced by high-intensity focused ultrasound (HIFU). At high-intensity exposure without overpressure, lesions have a tadpole, not cigar, shape (Watkin et al. 1996). Calculations and references were used to show that overpressure raises boiling temperature, increases the rate of dissolution of bubbles and restricts the amplitude of oscillation of bubbles in a sound field. References and measurement also indicate that overpressure has relatively little effect on other acoustic properties of water or excised tissue. Our experiments with B-mode US indicate the possible production of bubbles by HIFU. The dissipation time of a hyperechoic region produced by HIFU showed the same sensitivity to overpressure ($<$ 0.7 MPa) as did calculated dissolution times of a 30-μm bubble. Experiments in a high-pressure chamber (5.6 MPa) showed that the lesions were more cigar-shaped than lesions formed with no overpressure (0.1 MPa). The results were quantified as the ratio of the area of the near end of the lesion over the area of the far end. Ratios were 1.7 ± 0.3 at 0.1 MPa and 1.2 ± 0.2 at 5.6 MPa. Overpressure and its effect on bubbles seems likely to mitigate the distortion of the lesion shape.

Acknowledgements—The authors thank Schenk Packing Co. (Stanwood, WA) for their generous cooperation in providing bovine liver tissue, Murtuza Lokhandwalla and Prof. Bradford Sturtevant at the California Institute of Technology for lending us pressure chamber 2, Dr. Peter Kaczkowski and Fran Olson at Applied Research Laboratory (APL) for designing and building chamber 1, Dr. Pierre Mourad at APL for his encouragement and financial support of the project, Dr. Ian Rivens for help with preliminary experiments leading to this work and Dr. Naomi Fineberg of Indiana Medical School for help with the statistical analysis. The work was supported by a grant from DARPA/ONR.

REFERENCES

Akulichev V. Hydration of ions and the vacitation resistance of water. Sov Phys Acoust 1966;12:144.

Akulichev VA. Relationship of the pulsations of cavitation voids to the

emission of shock waves and cavitation noise. In: Rozenberg LD, ed. High-intensity ultrasonic fields. New York: Plenum, 1971:239–259.
Apfel RE. The role of impurities in cavitation-threshold determination. J Acoust Soc Am 1970;48:1179–1186.
Atchley AA. Acoustic cavitation and bubble dynamics. Physics. Oxford, MS: University of Mississippi, 1984:120.
Atchley AA, Frizzell LA, Apfel RE, et al. Thresholds for cavitation produced in water by pulsed ultrasound. Ultrasonics 1988;26:280–285.
Bailey MR, Cleveland RO, Sapozhnikov OA, et al. Effect of increased ambient pressure on lithotripsy-induced cavitation in bulk fluid and at solid surfaces. Collected Papers from the Joint Meeting "Berlin 99": 137th meeting of the Acoustical Society of America; 2nd convention of the European Acoustics Association; 25th German Acoustics DAGA conference, Berlin, Germany, Deutsche Gesellschaft fur Akustik (DEGA), 1999.
Bronskaya LM, Vigderman VS, Sokol'skaya AV, El'piner IE. Influence of the static pressure on ultrasonic chemical and biological effects. Sov Physics Acoust 1968;13:374–375.
Chavrier F, Chapelon JY, Gelet A, Cathignol D. Modeling of high-intensity focused ultrasound-induced lesions in the presence of cavitation bubbles. J Acoust Soc Am 2000;108:432–440.
Church CC. A theoretical study of cavitation generated by an extracorporeal shock wave lithotripter. J Acoust Soc Am 1989;86:215–227.
Clarke RL, ter Haar GR. Temperature rise recorded during lesion formation by high-intensity focused ultrasound. Ultrasound Med Biol 1997;23:299–306.
Cleveland RO, Sapozhnikov OA, Bailey MR, Crum LA. A dual passive cavitation detector for localized detection of lithotripsy-induced cavitation in vitro. J Acoust Soc Am 2000;107:1745–1758.
Crum LA. Nucleation and stabilization of microbubbles in liquids. Appl Sci Res. 1982;38:101–115.
Crum LA, Law W. The relative roles of thermal and nonthermal effects in the use of high intensity focused ultrasound for the treatment of benign prostatic hyperplasia. Proceedings of the 15th International Congress on Acoustics, Trondheim, Norway, 1995.
Curra FP, Mourad PD, Khokhlova VA, Crum LA. High intensity focused ultrasound and tissue heating: The effect of nonlinear sound propagation and vessel presence. Proc IEEE 1998;2:1419–1422.
Eller A, Flynn HG. Rectified diffusion during nonlinear pulsations of cavitation bubbles. J Acoust Soc Am 1965;37:493–503.
Epstein PS, Plesset MS. On the stability of gas bubbles in liquid-gas solutions. J Chem Phys 1950;18:1505–1509.
Frizzell LA, Carstensen EL, Dyro JF. Shear properties of mammalian tissues at low megahertz frequencies. J Acoust Soc Am 1976;60:1409–1411.
Fry FJ. Intense focused ultrasound in medicine. Eur Urol 1993;23:2–7.
Fry FJ. Ultrasonic visualization of ultrasonically produced lesions in brain. Confin Neurol 1970;32:38–52.
Fry FJ, Heimburger RF, Gibbons LV, Eggleton RC. Ultrasound for visualization and modification of brain tissue. IEEE Trans Sonics Ultrason 1970;SU-17:165–169.
Fry WJ, Mosberg WH, Bernard JW, Fry FJ. Production of focal destructive lesions in the central nervous system with ultrasound. J Neurosurg 1954;11:471–478.
Gelet A, Chapelon JY, Margonari J, et al. Prostatic tissue destruction by high-intensity focused ultrasound: Experimentation on canine prostate. J Endourol 1993a;7:249–253.
Gelet A, Chapelon JY, Margonari J, et al. High-intensity focused ultrasound experimentation on human benign prostatic hypertrophy. Eur Urol 1993b;23:44–47.
Gilmore FR. The growth or collapse of a spherical bubble in a viscous compressible liquid. Pasadena, CA: California Institute of Technology, 1952:1–40.
Hill CR. Ultrasonic exposure thresholds for changes in cells and tissues. J Acoust Soc Am 1971;52:667–672.
Holland CK, Deng CX, Apfel RE, et al. Direct evidence of cavitation in vivo from diagnostic ultrasound. Ultrasound Med Biol 1996;22:917–925.
Kargl SG, Williams KL, Lim R. Double monopole resonance of a gas-filled, spherical cavity in a sediment. J Acoust Soc Am 1998;103:265–274.
Lele PP. Effects of ultrasound on "solid" mammalian tissues and tumors in vivo. Ultrasound: Medical applications, biological effects and hazard potential. New York: Plenum, 1986:275–306.
Lizzi FL. High-precision thermotherapy for small lesions. Eur Urol 1993;23:23–28.
Lizzi FL, Coleman DJ, Driller J, et al. A therapeutic ultrasound system incorporating real-time ultrasonic scanning. 1986 Ultrasonics Symposium, Institute of Electrical and Electronic Engineers, New York, 1986.
Lynn JG, Zwemer RL, Chick AJ, Miller AF. A new method for the generation and use of focused ultrasound in experimental biology. J Gen Physiol 1942;26:179–193.
Meaney P, Cahill MD, ter Haar G. The intensity dependence of focused ultrasound lesion position. SPIE 1998;3249:246–256.
Meaney P, Cahill MD, ter Haar GR. The intensity dependence of lesion position shift during focused ultrasound surgery. Ultrasound Med Biol 2000;26:441–50.
Medwin H. Speed of sound in water: A simple equation for realistic parameters. J Acoust Soc Am 1975;58:1318–1319.
Nishi RY, Brown RF. Behavior of piezoceramic projector materials under hydrostatic pressure. J Acoust Soc Am 1964;36:1292–1296.
Pennes HH. Analysis of tissue and arterial blood temperatures in the resting human forearm. J Appl Physiol 1948;85:5–34.
Pohlhammer JD, Edwards CA, O'Brien JD Jr. Phase insensitive ultrasonic attenuation coefficient determination of fresh bovine liver over an extended frequency range. Med Phys 1981;8:792–794.
Press WH, Teukolsky SA, Vetterling WT, Flannery BP. Numerical recipes in Fortran. Cambridge, UK: Cambridge University Press, 1992:710–722.
Sanghvi NT, Fry FJ, Bihrle R, et al. Microbubbles during tissue treatment using high intensity focused ultrasound. IEEE 95 UFFC Sympos 1995:1249–1253.
Sonic-Technologies. Specifications manual for reference shock wave hydrophone. Hatboro, PA: Sonic-Technologies, 1994.
Sullivan DA. Historical review of real-fluid isentropic flow models. J Fluids Eng 1981;103:258–267.
ter Haar G. Ultasonically induced minimally invasive surgery. JEMU 1998;2:255–259.
Thompson PA. Compressible-fluid dynamics. Troy, NY: Rensselaer Polytechnic Institute, 1988:102.
Vaezy S, Shi X, Martin RW, et al. Real-time visualization of focused ultrasound therapy. Ultrasound Med Biol 2001;27 (in press).
Vaughan MG. High intensity focused ultrasound surgery of the prostate. MA Thesis, University of Melbourne. Melbourne, Australia 1993.
Vykhodtseva NI, Hynynen K, Damianou C. Histologic effects of high intensity pulsed ultrasound exposure with subharmonic emission in rabbit brain in vivo. Ultrasound Med Biol 1995;21:969–979.
Watkin NA, ter Haar GR, Morris SB, Woodhouse CR. The urological applications of focused ultrasound surgery. Br J Urol 1995;75(Suppl. 1):1–8.
Watkin NA, ter Haar GR, Rivens I. The intensity dependence of the site of maximal energy deposition in focused ultrasound surgery. Ultrasound Med Biol 1996;22:483–491.
Weast RC, ed. Handbook of chemistry and physics. Boca Raton, FL: CRC Press, 1985;D186–D187.
Wojcik G, Mould J Jr, Lizzi F, et al. Nonlinear modeling of therapeutic ultrasound. IEEE Ultrason Sympos 1995:1617–1622.
Yount DE. Skins of varying permeability: A stabilization mechanism for gas cavitation nuclei. J Acoust Soc Am 1979;65:1429–1439.